ICAS-88-1.5.3

DRIVING MECHANISMS IN UNSTABLE RAMJET COMBUSTORS

U. G. Hegde, D. Reuter and B. T. Zinn
Georgia Institute of Technology
Atlanta, Georgia 30332
U. S. A.

Abstract

This paper describes an investigation of combustion instability mechanisms in ramjet engines. Combustion instability occurs in a ramjet engine when the energy supplied by the combustion process excites one of the natural acoustic modes of the combustor. The research presented herein studies the unsteady behavior of a combination of V-shaped flames stabilized in a rectangular duct simulating a ramjet engine. By means of experimental and theoretical techniques it is shown that the instability is sustained by an intricate feedback loop connecting the acoustic oscillations, the unsteady combustion in the flame zone and vortex shedding at the flame holding region. A coupling exists between each pair of these three components of the feedback loop. The unsteady combustion drives the acoustic motions, the vortex shedding leads to unsteady combustion rates and, in turn, the vortex shedding is initiated by the acoustic oscillations.

Introduction

Recent developments of ramjet engines as part of integral rocket-ramjet propulsion systems have been hindered by the occurrences of destructive combustion instabilities[1]. These instabilities are characterized by either low frequency or high frequency pressure and velocity oscillations[1]. The low frequency rumble is in the range of 50- 500 Hz and is accompanied by longitudinal oscillations in the inlet section and the combustor or a combination of a longitudinal acoustic oscillation in the inlet section and a bulk mode type of oscillation in the combustor[2]. The high frequency screech occurs when one of the tangential acoustic modes of the combustor is excited. This type of instability can be often controlled by use of acoustic liners. At present, however, there is a lack of effective means for suppressing the low frequency type of instability because of insufficient understanding of the mechanisms responsible for its occurrence. This type of instability can, potentially, present serious problems because the interaction of the pressure oscillations with the inlet shock system may result in inlet unstarting and consequent loss of engine performance. In addition, excessive vibrational loads in the system may occur.

During the past four years an ongoing research program at Georgia Tech has been investigating this low frequency instability by studying the coupling mechanisms between the combustion process and gas dynamical oscillations in unstable ramjets. These mechanisms provide the energy required for the initiation and maintenance of the unstable oscillations. The research, conducted in a laboratory ramjet simulator, has found that driving of acoustic modes occurs via a complex interaction between acoustic wave oscillations, vortex shedding at the flame holding region and unsteady combustion in the vortices[3,4]. The precise coupling between these various facets of the driving mechanism is the focus of this paper.

In order to understand these couplings it is convenient at the outset to distinguish between acoustic motions associated with the combustion instability, vortical motions associated with the vortex shedding and the unsteady combustion. This may be accomplished by describing the unsteady fluid motions in an unstable ramjet in terms of a combination of three modes; that is, the potential or acoustic mode, the vortical mode and the entropy mode. This decomposition of fluid motion is well known in the literature[5,6]. Thus, the velocity vector, $\underset{\rightarrow}{v}$, is decomposed as follows

$$\underset{\rightarrow}{v} = \bar{\underset{\rightarrow}{v}} + \underset{\rightarrow}{v}' \; ; \; \underset{\rightarrow}{v}' = \underset{\rightarrow}{u}' + \nabla\phi \qquad (1)$$

where $\bar{\underset{\rightarrow}{v}}$ is the steady state component, $\nabla\cdot\underset{\rightarrow}{u}' = o$ and $\nabla \times \nabla\phi = o$.

It is shown elsewhere[6,7] that with the above flow description, the potential ϕ satisfies an acoustic wave equation and may, therefore, be identified with the acoustic field. On the other hand, $\underset{\rightarrow}{u}'$ describes the incompressible component of the velocity fluctuation and may be identified with the unsteady vortical field. This may be readily seen by noting that the unsteady vorticity, $\underset{\rightarrow}{r}'$, is given by

$$\underset{\rightarrow}{r}' = \nabla \times \underset{\rightarrow}{v}' = \nabla \times \underset{\rightarrow}{u}' \quad \text{as} \quad \nabla \times \nabla\phi = o \qquad (2)$$

For the purposes of this paper, the entropy mode will be identified with the unsteady combustion in the ramjet engine. The validity of this equivalence may be seen by writing the equation for the entropy, s, in the absence of diffusive processes

$$\frac{\partial s}{\partial t} + (\underset{\rightarrow}{v} \cdot \nabla)\, s = \frac{1}{\rho T}\dot{Q} \qquad (3)$$

where $\dot{Q}$, ρ and T are the rate of heat release by the combustion, the density and the temperature, respectively. Thus, when the heat release is zero the entropy is merely convected with the flow.

In the following development, the experimental ramjet apparatus and measurement techniques are first described briefly. This is followed by sections describing the coupling between the unsteady combustion and the acoustics, the coupling between the unsteady combustion and the vortical motions and finally, the coupling between the acoustic and vortical motions.

Experimental Apparatus

A schematic of the experimental apparatus, described in detail in earlier papers[3,8], is shown in Fig. 1. It consists of an injector through which a combustible mixture of propane and air at a maximum Reynolds number of 10000 is introduced into a 7.5x5 cm^2 rectangular duct which is 3 m

long. The combustor section is shown in more detail in Fig. 2. It consists of two symmetrically placed cylindrical flame holders each 6 mm in diameter. The two resulting V-shaped flames combine to form a W-shaped flame front. A flame merging zone may be identified in the central part of the combustor. The flame is quenched at the walls in the wall-flame interaction zones. The side walls of the combustor section are made of quartz enabling optical probing of the flame region. The burned gases flow out of the exhaust section. Both the combustor and exhaust sections are equipped with water cooled walls so that pressure transducers may be mounted directly at the walls to monitor the pressure oscillations at different locations. Acoustic drivers may also be installed in the exhaust section as shown in Fig. 1 to investigate the effects of imposed excitation on the flame. These forced excitation studies have been described in earlier papers[3,4] and will not be repeated here.

The following quantities have been measured:
(i) pressure oscillations at different locations along the duct by means of wall mounted transducers
(ii) C-H radiation from the flame. These have been measured from different narrow vertical slices of the flame to obtain a spatial distribution as well as from the flame as a whole to obtain the spatially integrated values. These measurements are indicative of the heat release rates from the flame[3,9].
(iii) axial and normal velocities. Both the steady state and time dependent fluctuations have been measured by means of Laser Doppler Velocimetry (LDV).
(iv) flame visualizations have been obtained by means of high speed and "phase locked" shadowgraphy techniques. The phase locked shadowgraphy is discussed in this paper.

Combustion - Acoustics Interaction

The flame configuration of Fig. 2 has been found to be highly unstable and results in levels of pressure oscillations exceeding 150 dB depending upon the fuel/air ratio. A representative pressure spectrum measured at the injector location is shown in Fig. 3. The presence of two peaks, at approximately 80 Hz and 160 Hz, is clearly seen in the spectrum. These frequencies correspond to the first and second natural longitudinal acoustic modes of the duct. It may be further noted that the component at 160 Hz is about 20 dB below the component at 80 Hz. This feature will be exploited in some of the experimental results to follow.

The corresponding spatially integrated C-H radiation (i.e., the heat release rate) spectrum is presented in Fig. 4. A strong similarity between Figs. 3 and 4 is evident; in particular, the presence of corresponding peaks at 80 Hz and 160 Hz. Thus, a strong connection between the acoustic pressure oscillations and the unsteady heat release from the flame may be expected.

A theoretical model of this interaction has been developed[9]. It predicts the pressure spectrum, S_{pp}, in terms of the measured spatially integrated radiation spectrum, S_{rr}. This relation may be expressed in the following form

$$S_{pp} = B \frac{\omega^2}{C_p^2} |G|^2 S_{rr} \qquad (4)$$

where G is a Green's Function which describes the acoustic response of the experimental setup to a unit source excitation, C_p is the specific heat at constant pressure, ω is the radian frequency of interest and B is a positive real constant which relates the measured radiation spectrum S_{rr} to the unsteady heat release rate spectrum S_{qq}; that is,

$$S_{qq} = B S_{rr} \qquad (5)$$

The two major assumptions involved in deriving Eq. 4 are: (a) the unsteady heat release from the combustion region is the dominant acoustic source in the experimental apparatus, and (b) the flame zone is compact as compared to the acoustic wavelengths of interest; that is,

$$\frac{L_f}{\lambda} \ll 1$$

where L_f and λ are the flame length and the acoustic wavelength of interest. This assumption restricts the validity of Eq. 4 to the low frequency end of the spectrum in the approximate range of 0 - 300 Hz. In the present studies the flame length was of the order of 10 cm whereas the acoustic wavelength of the first natural frequency of 80 Hz was of the order of 5 m, thus, satisfying the above length constraint. Further details regarding the derivation of Eq. 4 are provided in Ref. 9.

A comparison of the measured and theoretically predicted pressure spectrum at the injector end of the duct is presented in Fig. 5. The radiation spectrum of Fig. 4 has been used as the driving source S_{rr} in Eq. 4 for the pressure spectrum calculation. The agreement between the measured and predicted pressure spectra is excellent which corroborates the validity of assumption (a) above.

The coupling between the unsteady combustion in the flame region and the longitudinal acoustic motions is therefore clarified. The unsteady combustion acts as a strong source for the acoustic oscillations according to Eq. 4. It may be also shown that the Green's function G maximizes at the natural acoustic frequencies of the duct[9]. Thus, if a high unsteady combustion rate occurs at a frequency of a longitudinal acoustic mode of the system (for example, the first acoustic mode as in Fig. 4) then, the potential is present for the occurrence of longitudinal instabilities in the system.

Combustion - Vorticity Interaction

The next step in understanding the combustion instability mechanism is to elucidate the processes responsible for unsteady combustion in the flame region. As will be seen shortly, this occurs due to a strong interaction between the flame and the unsteady vortical field downstream of the flame holders.

First, the results of optical visualization of the flame region by means of "phase locked"

shadowgraphy are considered. The experimental setup is shown in Fig. 6. A laser beam passes through an expansion lens and a mechanical beam chopper before passing through the flame zone of the combustor. The temperature and density gradients in the flame zone result in a refractive index gradient which produces an image of the flame on the screen. As noted earlier, the oscillations are predominantly at the first natural frequency of the duct. This feature is exploited by operating the mechanical beam chopper at the frequency of the instability so that the laser beam illuminates the flame region at the same frequency. Thus, the image of the flame is obtained at approximately the same phase of the oscillation during each cycle. By comparing a signal from the beam chopper with the trace of the pressure oscillation, the phase of exposure of the shadowgraph may be obtained. This enables tracking of the flame shape and geometry during different phases of the oscillation.

A schematic of the flame region at different phases of one cycle of the oscillation at the first natural frequency is presented in Fig. 7. Here, θ represents the phase of the pressure oscillation with $\theta = 0^{o}$ representing the phase of maximum pressure. As is clearly evident, the flame shape is a strong function of the phase. For example, at $\theta = 0^{o}$, the two central flame branches are distinct and separate and they "merge" at a later time during the cycle. The presence of lobes in the flame structure is also evident. The size and position of these lobes is also a function of the phase.

An analysis of images similar to those shown in Fig. 7 revealed that as new lobes form at the flame holders and are convected downstream, the flame area (or in the two dimensional approximation, the flame length) also changes. The flame area is important in determining the unsteady combustion rates. This may be understood by noting that the reactants are consumed and products are formed at the flame surface. Thus, the extent of the flame surface determines the instantaneous reaction rate and hence the heat release rate. The variation in the flame length during a cycle of oscillation indicates, therefore, a variation in the heat release rate. Figure 8 presents this variation of the flame length as a function of the phase of the pressure oscillation. The flame length and the pressure oscillations are seen to be in phase. This means that the unsteady heat release rates are also in phase with the pressure oscillations indicating that Rayleigh's criterion[3,10] for the driving of acoustic waves by heat addition (i.e., the flame) is satisfied.

The characteristics of the lobes in the flame structure, which ultimately result in an unsteady heat release rate, have been further investigated by using an LDV system to measure the velocity field in the flame region. Full details are provided in Ref. 11. Here, it will be demonstrated that the lobes are caused by the action of unsteady vortices shed from the flame holders.

The unsteady vorticity, r', is given by

$$r' = \frac{\partial v'}{\partial x} - \frac{\partial u'}{\partial y} \qquad (6)$$

where u' and v' are the unsteady velocity fluctuations in the x (axial) and y (normal) directions. The unsteady vorticity may be experimentally determined by finite differencing Eq. 6 using the measured unsteady velocity components u' and v'.

The characteristics of the region downstream of the lower flame holder are described in Fig. 9. The x-axis corresponds to the distance downstream of the lower flame holder and the zero location on the y-axis is the position of the lower flame holder. The phase of the pressure in this figure is $\theta = 0^{o}$ (that is, the phase of maximum pressure). The location of the flame front, obtained by means of the shadowgraphy technique described earlier, is superimposed on the figure.

It was found[11] that one cycle of the pressure oscillation corresponds to one cycle of vortex shedding; that is, during one cycle, one positive (anticlockwise) and one negative (clockwise) vortices are shed from both the top and bottom sides of the flame holder. Moreover, this shedding is symmetric. For example, regions of positive and negative vorticity, marked A and B, respectively, are clearly seen downstream of the lower flame holder. These vortices have been shed from the top surface of the flame holder. The flame front at the interface between these two vortices is distorted by the action of these vortices and forms a "kink". This "kink" separates one lobe of the flame front from the adjoining one. It is evident, therefore, that the lobes in the flame arise as a consequence of the unsteady vortex shedding at the flame holder.

Thus, it is clear that the unsteady vortex shedding at the flame holder causes a periodic distortion of the flame surface. This results in the appearance of the lobes in the flame and the cyclic variation of the flame area and the reaction and heat release rates. The unsteady combustion at the frequency of instability arises, therefore, as a result of the coupling between the flame and the unsteady vortical field.

Acoustic - Vorticity Interaction

It has been noted that one cycle of the vortex shedding coincides with one cycle of the acoustic pressure oscillation. This suggests a locking in of the vortex shedding with the acoustic oscillations and represents the third component of the feedback loop connecting the acoustic oscillations, the unsteady combustion and the vortical field.

The presence of unsteady vortex shedding at the flame holder suggests an instability of the shear layer which forms in the wake of the flame holder[4]. This shear layer is extremely complex involving gradients in both the velocity and temperature. In addition, the combustion processes further affect its development. As a first step in understanding the interaction between the acoustic and vortical modes, the authors of this paper have investigated theoretically the instability of a shear layer with temperature and density gradients in a similar configuration[7]. In this analysis, the combustion processes are not accounted for; nevertheless, it is believed that salient features of the acoustic-vorticity interaction are

clarified.

As the unsteady vortical velocities are incompressible (see Eq. 1), a stream function, ψ, may be defined such that

$$v' = \frac{\partial \psi}{\partial x} \quad \text{and} \quad u' = -\frac{\partial \psi}{\partial y}$$

It may be further shown that ψ can be written as the sum of two components ψ_1 and ψ_2; that is,

$$\psi = \psi_1 + \psi_2$$

where ψ_1 corresponds to the inherently unstable vortical mode of the shear layer which depends only on the steady velocity, temperature and their gradients. The component, ψ_2 on the other hand, also depends on the acoustic motions interacting with the shear layer. These acoustic motions are described in terms of the potential ϕ (see Eq. 1). Under conditions of shear layer instability, the component ψ_1 corresponds to a spatially growing vortical wave whereas the component ψ_2 does not exhibit any spatial growth.

The connection between ψ_1 and ψ_2 represents the interaction between the acoustic and vortical motions and it arises because at the shear layer origin an initial condition on the vortical velocities must be satisfied. This initial condition will, in general, depend upon the actual configuration of the flow. For example, for a flow leaving a sharp trailing edge the normal velocities at the trailing edge must vanish if the flow is to remain parallel. This condition sets the initial magnitude and phase of the unstable vortical wave, ψ_1, in terms of the acoustic motions described by the acoustic potential ϕ (see Eq. 1). Further downstream, due to spatial growth, the unstable vortical wave, ψ_1, dominates the component ψ_2 and the interactions between the two become negligible.

It is believed that a similar process occurs in the experimental ramjet simulator. That is, the acoustic motions trigger a fluid dynamic instability of the shear layer formed in the wake of the flame holders. The subsequent roll up of the shear layer leads to the formation of the observed unsteady vortices and heat release processes.

Conclusion

The driving mechanisms for longitudinal combustion instabilities in ramjet engines have been investigated in a laboratory simulator. It has been found that the instabilities arise via an intricate interaction between the acoustic, vortical and entropy modes of the fluid motion. The unsteady combustion in the flame region drives the acoustic oscillations associated with the combustion instability. The unsteady combustion results from the action of unsteady vortices shed at the flame holders. These vortices periodically distort the flame resulting in oscillations of the heat release rates. The vortex shedding, in turn, is initiated by the acoustic motions interacting with the shear layer formed in the wake of the flame holders. Thus, the combustion instability is driven and sustained by means of a feedback loop connecting the unsteady combustion, the acoustic oscillations and the vortex shedding at the flame holders.

Acknowledgement

This work has been supported under U. S. Navy Contract No. SFRC No. N00014 - 84 - K - 0470.

References

1. Waugh, R. C. and Brown, R. S., "A Literature Survey of Ramjet Combustor Instability", CPIA Publication No. 375, pp. 1-13, 1983.

2. Rogers, T., "Ramjet Inlet/Combustor Pulsations Study", Final Report, Naval Weapons Center, S-1463A, Setp. 1977 - May 1978.

3. Hegde, U. G., Reuter, D., Daniel, B. R. and Zinn, B. T., "Flame Driving of Longitudinal Instabilities in Dump Type Ramjet Combustors", Combustion Science and Technology, Vol. 55, pp. 125- 138, 1987.

4. Hegde, U. G., Reuter, D., Daniel, B. R. and Zinn, B. T., "Fluid Mechanically Coupled Combustion Instabilities in Ramjet Combustors", AIAA Paper No. 87-0216, January 1987.

5. Chu. B. T. and Kovasznay, L. S. G., "Non-Linear Interactions in a Viscous Heat Conducting Compressible Gas", Journal of Fluid Mechanics, Vol 3, 1958.

6. Yates, J. E. and Sandri, G., "Bernoulli Enthalpy: A Fundamental Concept in the Theory of Sound",in Aeroacoustics: Jet Noise, Combustion and Core Engine Noise (Ed: I. R. Schwarz), M. I. T. Press, 1976.

7. Hegde, U. G. and Zinn, B. T., "Vortical Mode Instability of Shear Layers with Temperature and Density Gradients", submitted to AIAA Journal.

8. Hegde, U. G., Reuter, D. and Zinn, B. T., "Combustion Instability Mechanisms in Ramjets", AIAA Paper No. 88-0150, January 1988.

9. Hegde, U. G., Reuter, D. and Zinn, B. T., "Sound Generation By Ducted Flames", To be published in AIAA Journal.

10. Lord Rayleigh, "The Theory of Sound", Vol. II, pp. 224-235, Dover, 1945.

11. Reuter, D. M., Hegde, U. G. and Zinn, B. T., "Flowfield Measurements in an Unstable Ramjet Burner", AIAA Paper No. 88-2855, July 1988.

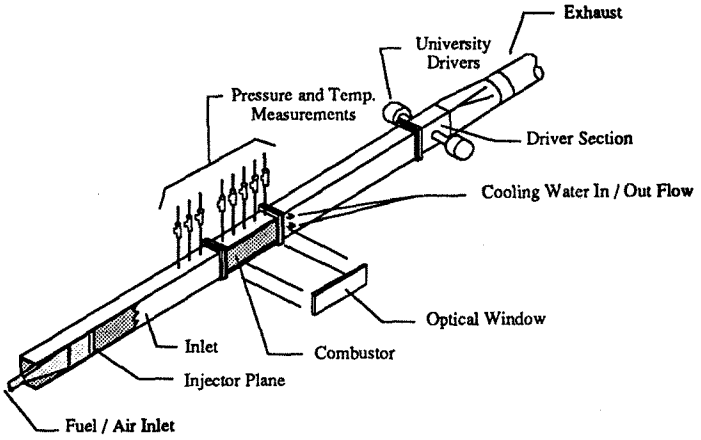

Fig. 1. Schematic of the Developed Experimental Apparatus.

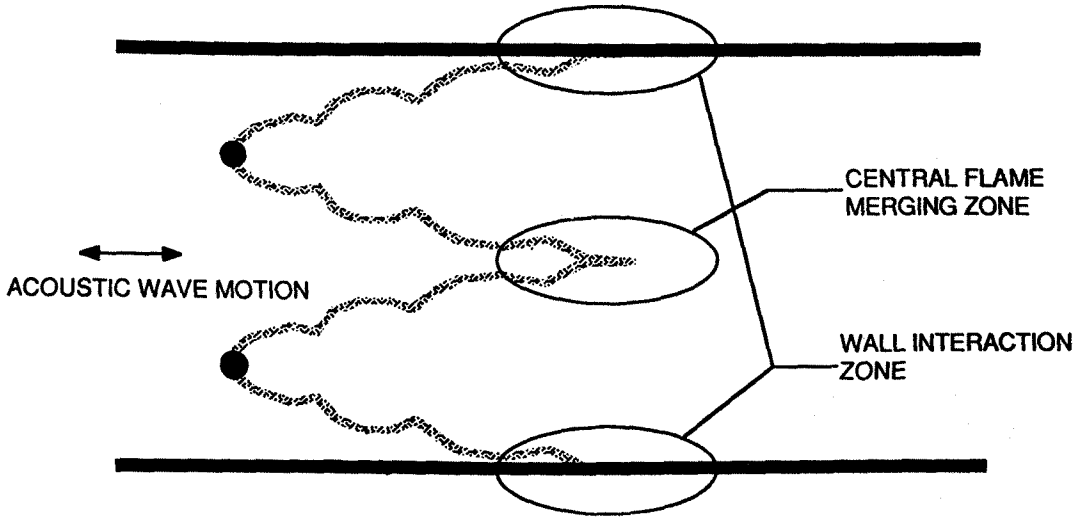

Fig. 2. Flame Geometry in the Combustor.

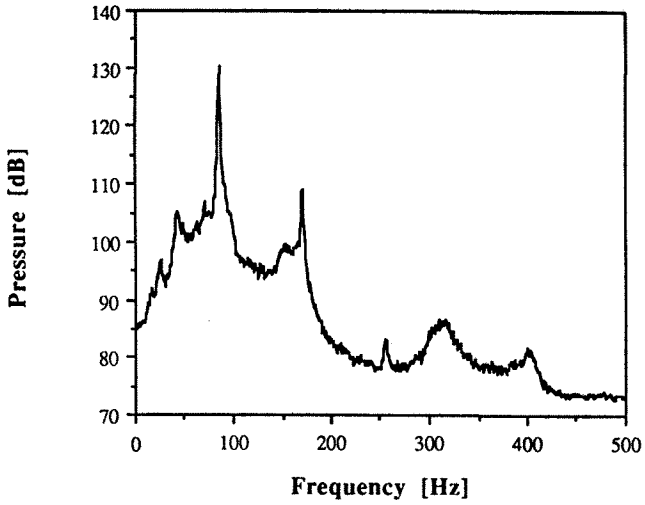

Fig. 3. Measured Pressure Spectrum at the Injector.

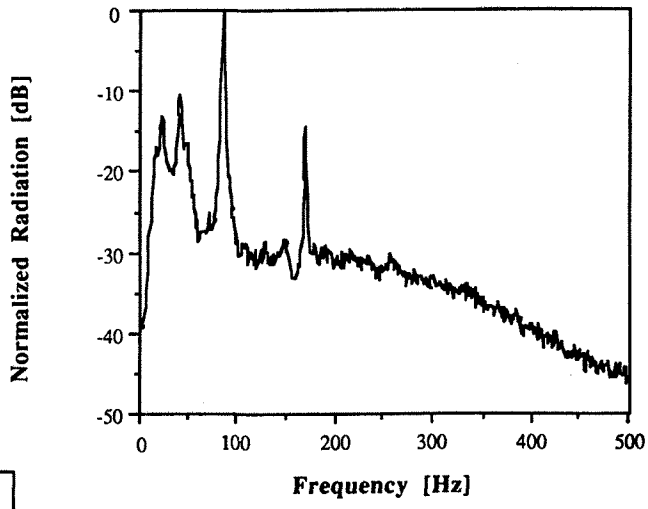

Fig. 4. Spatially Integrated C-H Radiation Spectrum.

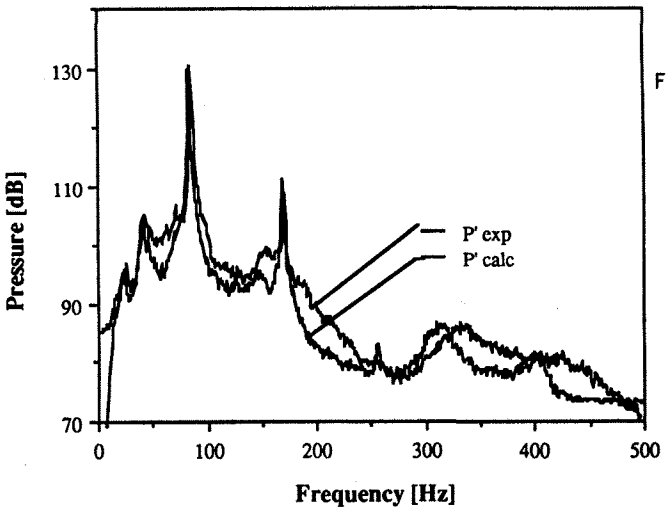

Fig. 5. Comparison of Experimental and Theoretical Pressure Spectra at the Injector.

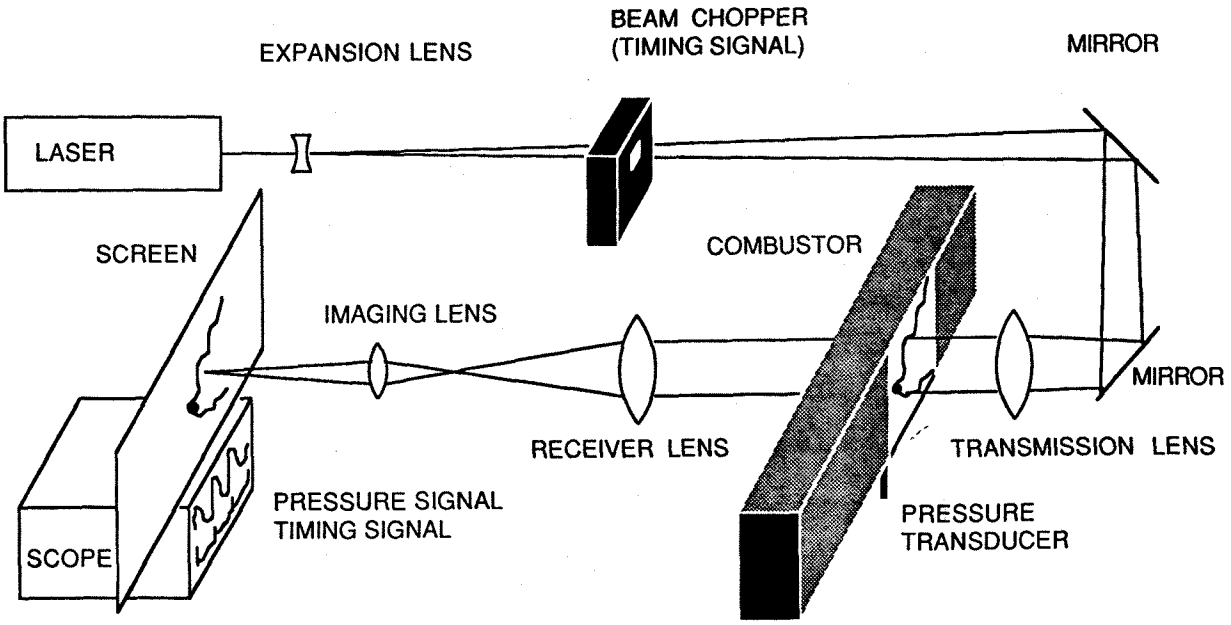

Fig. 6. Schematic of the Experimental Technique Utilized For "Phase Locked" Shadowgraphy of the Flame Region.

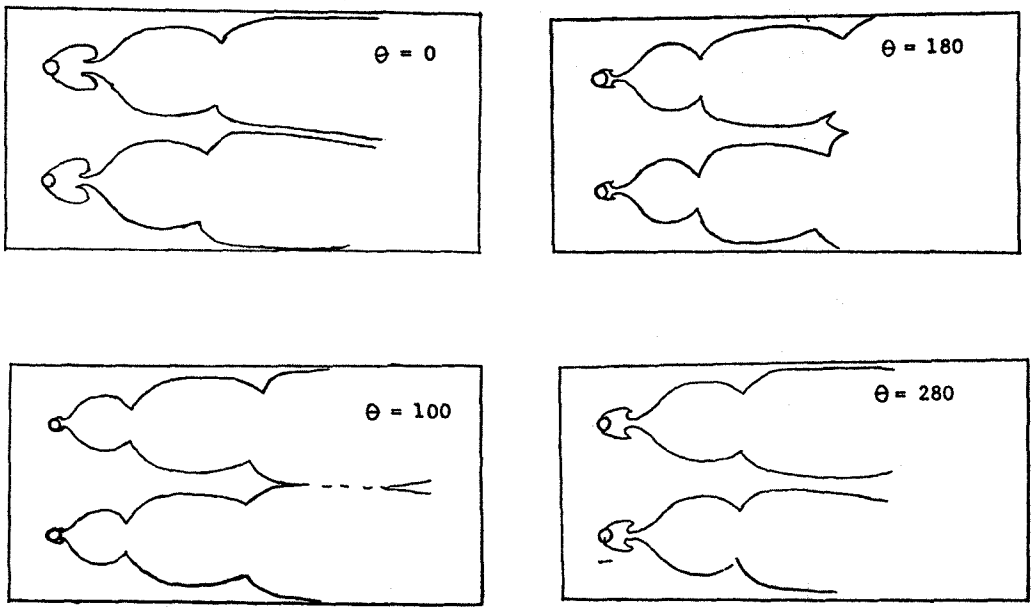

Fig. 7. Schematic of the Flame Shapes at Different Phases of A Cycle of Oscillation. $\theta = 0^{o}$ Represents the Phase of Maximum Pressure.

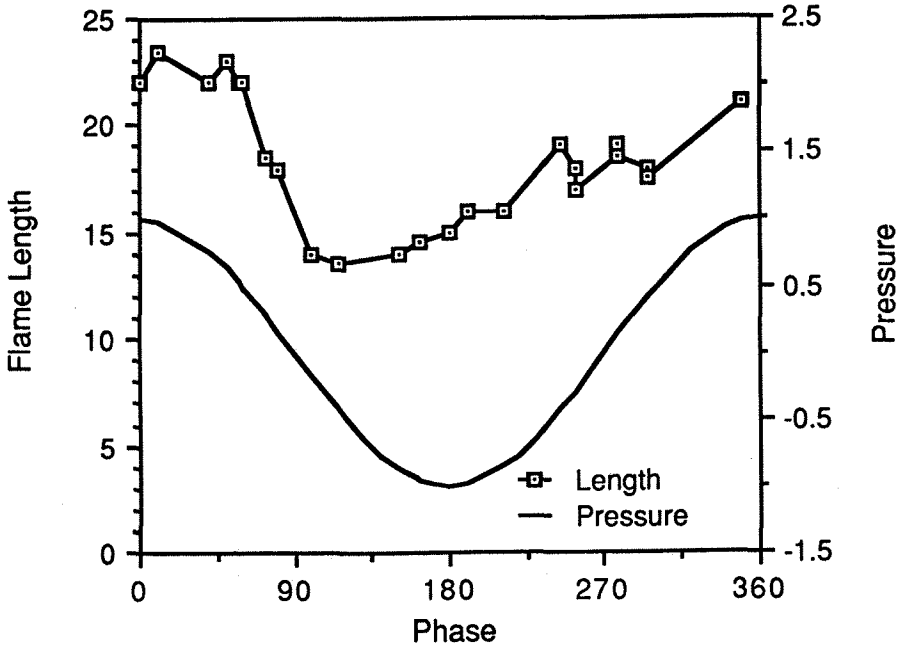

Fig. 8. Flame Length and Pressure Oscillations As a Function of the Phase of the Pressure Oscillation.

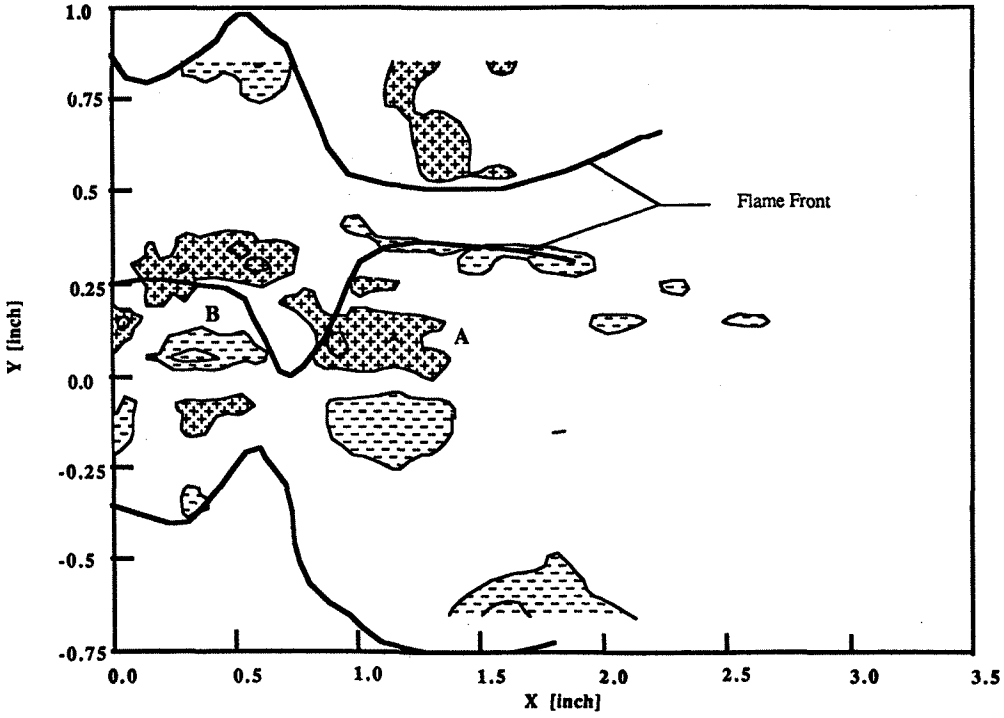

Fig. 9. Measured Unsteady Vorticity Downstream of the Lower Flame Holder. + Anti-clockwise Vorticity. - Clockwise Vorticity.